NASA Technical Memorandum 87193

Validation of Viscous and Inviscid Computational Methods for Turbomachinery Components

Louis A. Povinelli
Lewis Research Center
Cleveland, Ohio

Prepared for the
31st International Gas Turbine Conference and Exhibition
sponsored by American Society of Mechanical Engineers
Dusseldorf, West Germany, June 8-12, 1986

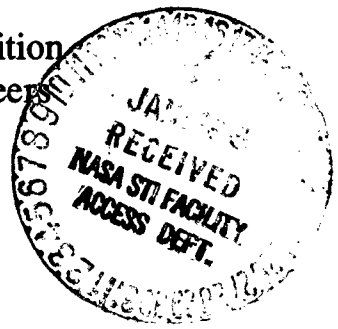

NASA

VALIDATION OF VISCOUS AND INVISCID COMPUTATIONAL METHODS FOR TURBOMACHINERY COMPONENTS

Louis A. Povinelli
National Aeronautics and Space Administration
Lewis Research Center
Cleveland, Ohio 44135

ABSTRACT

An assessment of several three-dimensional computer codes used at the NASA Lewis Research Center is presented. Four flow situations are examined, for which both experimental data and computational results are available. The four flows form a basis for the evaluation of the computational procedures. It was concluded that transonic rotor flow at peak efficiency conditions may be calculated with a reasonable degree of accuracy, whereas, off-design conditions are not accurately determined. Duct flows and turbine cascade flows may also be computed with reasonable accuracy whereas radial inflow turbine flow remains a challenging problem.

INTRODUCTION

The design and analysis of future propulsion system components will require greater analytical sophistication than is currently employed. This increase in sophistication is needed because component design is becoming more complex as newer features are being incorporated into engines. These newer features include items such as leaning, bowing, sweeping, and contouring of vanes and blades. These features, in combination with lower blade aspect ratios will lead to more complicated flows within the engine components, i.e., strong secondary flow motion. The secondary motion will cause a higher uncertainty in the heat transfer to the walls and blade surfaces. More fundamental knowledge of the flow will be required for effective design, including such items as the state of the boundary layer, location of transition, and the effect of turbulence on transition and heat transfer. Stator-rotor interactions and associated unsteady flow fields is also an important area that requires far greater understanding. The proper description of the initial flow conditions entering the engine component must also be understood, measured and modeled. It is believed that if these complex phenomena are to be modeled and computed, it will be necessary to develop three-dimensional viscous codes. A substantial amount of effort will be needed to develop, assess, refine, and apply such numerical techniques. The return, however, in terms of improved performance and heat transfer predictions makes the effort worthwhile.

The current industrial approach to the design and analysis of turbomachinery is to rely on inviscid computations coupled with boundary layer calculations and a variety of loss correlations. Designers have learned how to design and analyze turbomachinery very successfully using that approach as long as the new designs lie within the range of the empirical data base employed.

At the twenty-ninth ASME International Gas Turbine Conference, an assessment of the design procedure described above was presented by this author (1) for turbine aerodynamic computations used at the Lewis Research Center. The scope of this paper is to summarize the results obtained from the comparison of numerical computations and experimental data for a number of other propulsion system components, i.e., compressors, ducts, radial turbines, and cascades. For purposes of assessment, attention is focused on flow field computations using the inviscid computer codes TSONIC/MERIDL and BLAYER (2), the Denton code (3-5), and the viscous codes PEPSIG (6-8), and MINT (9). Comparisons are presented of the computer results with experimental data obtained from a transonic fan (10,11), a transition duct (12,13), a radial turbine (14,15), and a rectilinear cascade (16). Although Ref. 14 does not contain experimental data, it is illustrative of the trend toward more sophisticated design concepts. The method or approach used to carry out the assessment of the computations is presented in the following section.

APPROACH

The approach used in this paper is to examine a number of experimental studies for which selected aerodynamic parameters have also been computed and to arrive at conclusions regarding our predictive capability. Four experiments and the corresponding computations will be examined sequentially. A brief description of each study will be presented, including, as appropriate, the design conditions, the experimental measurements, the inviscid or viscous flow computations, the boundary layer computations and the loss calculations. Each of the four studies were examined as to adequacy of the computational scheme to predict the experimental data. On the the basis of the comparison, an evaluation or assessment of the predictive capability of the computer code will be presented. Additionally, potential problems associated with the computational method will be identified. Specific examples will also be discussed regarding the need for additional code verification. The four flow examples chosen for study involved an examination of:

(1) Mach number variation in a transonic fan rotor (10)

(2) Streamwise and secondary velocities in a transition duct (12)

(3) Rotor exit flow angles and total pressure ratio in a radial turbine (15)

(4) Pressure and velocity variations in a rectilinear cascade (16).
These four flow examples will now be discussed sequentially in the RESULTS section.

RESULTS

Transonic Fan Flow (10)

Rotor design. The compressor rotor was the first stage rotor of a NASA Lewis designed two-stage fan. The first rotor was designed as a 22-blade, low-aspect ratio (1.56), damperless replacement for an original 43-blade, high-aspect ratio (2.94), damped rotor. The new blading exhibited a total pressure ratio of 1.629 and an adiabatic efficiency of 0.896, when tested in the two-stage configuration. At the design tip speed of 428.9 m/s and design flow rate of 33.25 kg/s, the inlet relative Mach number was 1.38 at the rotor tip. The data to be discussed in this paper deals only with single rotor operation at either the peak efficiency point or the near stall condition.

Rotor static pressure rise. The numerical computations were performed using the procedure described in Refs. 4 and 5, including the simulation of boundary layer effects. Total pressure, temperature, tangential velocity, and meridional flow angle were specified approximately one chord upstream. The properties were held constant at each spanwise grid line and assumed uniform in the tangential direction. The static pressure at the hub was the only downstream condition imposed. The computational grid used was 21 (pitch) by 11 (span) by 95 (axial). The results of the computation are shown in Fig. 1 for both the hub and tip locations. The analysis without boundary layers predicted a higher rise in static pressure than was measured; whereas, the analysis with boundary layers shows excellent agreement with the measured data. The agreement spans the range of mass flow from near stall to peak efficiency to maximum flow. On an absolute basis, the predicted and calculated mass flows agreed to within 0.06 percent for the max flow case.

Relative Mach number. A fringe laser anemometer system was used in a back-scatter mode with fluorescent seed particles to measure flow velocities and angles in the rotor flow field. Figure 2 shows a composite of the experimentally derived Mach number and the inviscid computations at various chordwise locations. The comparison is at the 30 percent span position and is for three flow conditions, i.e., maximum flow, peak efficiency, and near stall. The shock locations are shown for each flow rate in order to provide a picture of the flow in the passage. The laser data in Fig. 2 shows the progression from an oblique shock at max flow with supersonic flow in the aft portion of the blading, to a near normal shock followed by a second shock at peak efficiency, and finally, a single normal shock upstream of the blade leading edge at the near stall point. The results obtained with the three-dimensional analysis code are also shown in the figure. For the max flow case, the major difference between experiment and analysis is the location of the second shock at the exit of the passage. The agreement at the peak efficiency point between the data is much better than for the max flow case. The front shock is accurately located by the code and there is a rear shock predicted in approximately the same position as the measured rear shock. The rear shock extends from the pressure surface to about the midpitch position.

For the near stall condition, the agreement between analysis and data is good in terms of shock location and peak Mach number. A quantitative comparison of the results is shown in Fig. 3. The relative Mach number along a midpitch line is plotted versus percent chord at 30 percent span for all three operating points. For the max flow case, the expansion of the flow after the first shock, as predicted by the analysis, leads to a strong passage shock at 70 percent chord. Some indication of a second shock in the max flow laser data is evident from the peak in Mach number at 10 percent chord, plateau from 30 to 40 percent chord and subsequent deceleration from 40 to 60 percent chord. Reasonable agreement between the analysis and experiment is seen for the first shock location. However, the second shock location shows poor agreement as does the magnitude of the predicted Mach numbers for chord positions greater than 35 percent.

The agreement between analysis and data is good for the peak efficiency case. The analysis does not clearly indicate the presence of two shocks in the system as indicated by the data at 10 and 60 percent. The predicted Mach number is somewhat low relative to the data for chord positions greater than 50 percent. For the near stall conditions, the Mach number was significantly underpredicted for values greater than 10 percent; but the shock location occurs at the "experimentally correct" location.

Figure 4 shows the variation in Mach number close to the blade pressure and suction surfaces for three spanwise positions for both the peak efficiency and the near stall flow cases. For all three spanwise locations, the agreement of blade loading between analysis and data is relatively good for the peak efficiency case. For the near stall condition, the analysis yields higher loadings at 10 and 30 percent, but is reasonably good at 70 percent. Generally, the increased loading results from an underprediction of the Mach number on the pressure surface. Although the shock locations are predicted fairly well, the Mach number predictions for the 10 and 30 percent span positions are subsonic compared to the supersonic experimental data.

Assessment of analysis. The results obtained from the three-dimensional Euler code coupled with a boundary layer correction were found to predict the static pressure rise across a transonic rotor with a high degree of accuracy. Prediction of the first shock location on the midpitch plane was reasonably predicted for the max flow, peak efficiency, and near stall cases at 30 percent span. Peak Mach number was also well predicted. However, the second shock location prediction was not accurate for the max flow case. Also the magnitude of the computed Mach number was found to vary considerably for both the near stall and max flow cases. Predictions for the Mach number on the pressure and suction surfaces of the blading for the peak efficiency case was accurate at all spanwise locations. The near stall condition, however, yields large Mach number discrepancies between computations and laser measurements.

It is observed that the inviscid analysis yielded the best agreement with data for the flow field with a single oblique shock wave, e.g., near the suction surface for the peak efficiency case. For an oblique shock followed by a weak shock, the agreement is less satisfactory, such as observed along the pressure surface for the peak efficiency case. When the oblique shock is followed by a strong passage shock, the inviscid analysis does not predict the double shock structure very well (max flow condition). In the

presence of a strong normal shock, which may lead to blade surface separation, the analysis also shows poor agreement with data (near stall condition). These results suggest limitations on the analysis relative to flow angle and Mach number changes in the presence of flow discontinuities. The assessment of this inviscid analysis has been made on the basis that the experimental laser data correctly represented the flow phenomena throughout the entire flow field. At this time, some unresolved questions remain regarding the measurements in the vicinity of shock waves. The uncertainty is associated with signal conditioning required in the near shock regions and subsequent biasing of the measurements by the larger particles (1.4 μm). Further assessment is dependent on subsequent experimental measurements.

It is concluded that the Euler analysis described above accurately predicts the loading, first shock location, and peak Mach numbers extremely well for the peak efficiency flow case. For other mass flow conditions, i.e., near stall or maximum flow, the analysis yields an overall performance number of high accuracy but does not capture the flow structure accurately.

Transition Duct (12)

Duct configuration. The circular cross-section, S-duct geometry analyzed is shown in Fig. 5 and consisted of two 22.5° circular arc bends. The ratio of the centerline radius to the cross-section diameter was seven. This type of geometry with modest curvature is typical of propulsion system ducting and could precede the turbomachinery. Computations were made for laminar and turbulent flow cases. For the laminar flow, the Reynolds number based on cross-section diameter was 790 and the Dean number was 211. The Dean number is defined as the product of the Reynolds number and the square root of the ratio of cross sectional radius to the radius of curvature. For the turbulent case, the Reynolds number was 48,000 with a corresponding Dean number of 12,828. The grids used were 20 by 20 by 80 for the laminar, and 50 by 50 by 80 for the turbulent flow. Computer solutions were carried out using the parabolized Navier-Stokes code, PEPSIG, described in Refs. 6 to 8, which was a joint effort with the Lewis Research Center and Scientific Research Associates, Inc.

Streamwise velocity. Secondary flows are generated in both bends of the duct, resulting in the concentration of vortex motion at the top of the duct as the flow approaches the exit. The effect of the secondary flow on the stream-wise flow is shown in Fig. 6. The boundary layer along the bottom of the duct initially thickens due to an adverse pressure gradient. At the second station, the secondary flow has caused the boundary layer in the top half to thicken significantly. Through the inflection region, the analysis predicts a small region of separation. A "FLARE" approximation (17) which assumes a small change in the zero wall velocity position was used to allow the streamwise marching analysis to continue. In the second half of the duct, the concentration of the vortices near the top causes significant distortions. The secondary flow near the wall in the bottom half causes boundary layer thickening. Fig. 7 shows a comparison of the computed streamwise velocity profiles with experimental data. Reasonable agreement is observed up to the 20.25° position. In the second half of the duct, where severe flow distortions occur as well as flow separation, the agreement is not as good, especially on the top half of the duct. An additional fine mesh calculation does not improve the comparison. The turbulent computations are shown in Fig. 8. The boundary layers are observed to be thinner than for the laminar case, which results in lower secondary velocities. Also, the vortices are more concentrated and located nearer the top of the duct. Figure 9 shows the computed and experimental streamwise velocity profiles. Reasonable agreement is also obtained for the turbulent case up to the 20.25° position. In the second half of the duct, the agreement is poor. However, mesh resolution was found to have a strong effect on the results and reasonable agreement is observed with the 50 by 50 by 80 grid. With the coarser grid, the thin boundary layers and secondary flow vortices are not resolved well enough for the analysis to predict the distorted flow region.

Assessment. The PEPSIG analysis qualitatively predicted the flow phenomena occurring within an S-shaped duct with both laminar and turbulent flow. In the laminar flow case, the thick boundary layer leads to large regions of secondary flow near the exit of the duct. It is precisely in this region that the largest discrepancy occurs between the parabolized solver and the experimental data. With thinner boundary layers in the turbulent flow, the secondary flow is more concentrated and the comparison with analysis is somewhat improved. The improvement, however, was achieved only with significantly higher resolution of the computational grids. With thin boundary layers, 50 by 50 cross-sectional meshes are required to resolve the flow motion. In the laminar flow, cross-sectional grids of 20 by 20 were sufficient. It is concluded that the parabolized marching code provides a reasonably accurate analysis of turbulent subsonic flow in turning ducts of modest curvature. Further refinements are required in order to achieve quantitative agreement for flows with thicker boundary layers where the extent of secondary flow motion is much larger.

Radial Turbine (15)

Turbine rotor design. The radial turbine analyzed had a 15 cm tip diameter radial-inflow rotor, and is described in Ref. 18. The rotor had 12 blades which were sufficiently thick to allow internal cooling passages and the trailing-edge ejection of coolant. The rotor had unswept radial blades at the inducer inlet and large blockages resulting from the thick trailing edges. The experimental program was undertaken to obtain performance and an external loss breakdown. Hence, no measurements were obtained within the rotor blading, but the results of rotor inlet and exit surveys were obtained.

Rotor exit flow angle. The three-dimensional Euler code described in the Transonic Fan Flow section was used for these computations. The input data used to run the code was the blade geometry, absolute flow angle at the rotor inlet, total pressure and temperature at the rotor inlet, the hub static pressure at the rotor exit, and the rotational speed. The computational grid was packed near the blade surfaces in addition to the streamwise grid packing around the leading and trailing edges. Cusps were used at the edges to reduce entropy and total pressure changes due to errors in finite-differencing schemes around these regions. The computational meshes in the leading edge region are shown in Fig. 10. The rounded leading edge geometry in Fig. 10(b) more closely approximates the test hardware. The computed three-dimensional variation in rotor exit flow angle was

circumferentially averaged at each grid location between hub and shroud. The radial distribution of these averaged absolute flow angles were then compared with the experimental data, see Fig. 11. Figure 11(a) shows the effect of the two leading edge cusps on the rotor exit flow angle calculation. Neither one of the leading edge meshes yields sufficient turning of the flow over the lower 40 percent of the annulus height. Figure 11(b) shows the effect of a 2° reduction in the rotor inlet absolute flow angle for the blunt leading edge case. In this case, the rotor exit flow angles are overturned relative to the experimental values in the outer portion of the annulus and underturned in the inner 30 percent of the annulus.

Total pressure ratio. The computed ratio of rotor-exit-to-turbine-inlet total pressure was also compared to experimental data by circumferentially mass-averaging the calculations at each grid location between hub and shroud. Figure 12(a) shows the comparison for both the rounded and blunt leading edge computations with the experimental data. Additional grid refinements did not improve the comparison. Generally, the calculated pressure ratios are underpredicted relative to the experimental data. Figure 12(b) shows the effect of reducing the rotor inlet absolute flow angle toward optimum incidence by 2°. With this reduction, the calculated total pressures are at about the same level as the viscous experimental flow.

Assessment. The three-dimensional inviscid analysis yielded exit flow angles that are substantially underturned relative to the experimental data, especially near the hub surface. This result might be anticipated in view of the fact that flow separation and wake formation will occur in the actual turbine due to large trailing-edge blockage (approximately 79 percent at the hub). These effects are not included in the inviscid analyses, and the flow is diffused without separation in the calculations. Likewise, viscous boundary layer separation and endwall vorticity are important factors near the blade leading edge which are absent in the analysis. The total pressure was under-predicted relative to data. However, on an overall basis, the computed pressure ratio averaged over the annulus agreed well with data when the absolute inlet angle was reduced by 2°.

On the basis of the results obtained, it is concluded that the highly loaded and stressed radial turbine blade with its blunt leading and trailing edges are insufficiently modeled with inviscid analyses. Blades with more rounded leading edges, similar to an axial turbine, or the thin fan blade discussed earlier may be more amenable to analysis.

Rectilinear Cascade (16)

Cascade geometry. The cascade investigated in this flow example was the two-dimensional, low-solidity Allison C3X axial turbine vane (19) and a corresponding three-dimensional rectilinear version of the C3X cascade. The latter configuration consisted of a C3X cascade situated in the azimuthal-radial plane, and bounded in the transverse direction by an endwall and a symmetry plane. The three-dimensionality resulted from stacking similar planes parallel to each other in the direction normal to a fixed endwall. Experimental data for the two-dimensional cascade included aerodynamic measurements with and without film cooling.

Pressure distribution. Computations for the cascade were carried out with a time-dependent, ensemble-averaged Navier-Stokes code using an "O" grid consisting of 100 by 25 by 15 points in the azimuthal, radial and transverse directions. The computations were initiated with an inlet Mach number of 0.15, Reynolds number (inlet freestream conditions) of 730, and ratio of inlet total to downstream exit static pressure of 1.95. Excellent agreement was obtained between experimental data and computations for the two-dimensional case and for clarity, the results are shown as single solid lines in Fig. 13. The three-dimensional laminar results are shown in Fig. 13 for different heights above the endwall. On the pressure side, the distribution shows the same values as the two-dimensional result. However, on the suction side, a difference of as much as 15 percent over the two-dimensional result is observed. The pressure difference persists away from the endwall up to a value of some 26 percent span, where the pressure values approach the two-dimensional results. These variations indicate a spanwise blade loading change and are consistent with the formation of large secondary flow regions, i.e., horseshoe and passage vortices. Figure 14 shows the velocity vector plots near the cascade leading edge for two spanwise locations. The flow near the endwall, Fig. 14(a), shows the existence of a saddle point, a phenomena which is a precursor to flow dividing and vortex formation. At the midstream position, the saddle point has disappeared and a stagnation point forms on the nose of the blade surface.

Assessment. The two-dimensional pressure predictions from the compressible Navier-Stokes code were found to be in good agreement with experimental cascade data. In addition the calculations duplicated most of the features associated with turbine cascade flow fields. Flow-turning, leading edge stagnation region, and boundary layer development were observed in the computations. These results demonstrate the ability of the MINT code to compute blade surface pressure distributions and viscous flow development. Additional assessment requires experimental data for this vane configuration at various spanwise positions. In addition, continuation of this code development is required in order to demonstrate a turbulent cascade calculation. In order to achieve those goals, it will be necessary to continue work on laminar-turbulent transition as well as determining a suitable turbulence model. The development of three-dimensional viscous computational codes appears to be essential to the improvement of turbomachinery design methods.

CONCLUSIONS

Comparison between measured and computed aerodynamic parameters have been examined in an effort to evaluate current computational capabilities. Specifically, the ability of the inviscid Denton code coupled with a boundary layer approximation to compute rotor Mach number distributions was examined. It was concluded that the computational procedure reasonable predicts the loading, first shock location, and peak Mach number for the peak efficiency operating point. It was further concluded that for the near stall and maximum flow conditions, the Euler code predicts overall performance, but does not replicate the flow structure accurately.

The second evaluation was carried out for internal duct flow of modest curvature for which experimental laser measurements of velocity were available. These

data were compared with the results of the parabolized Navier-Stokes code, PEPSIG. It was concluded that this code predicted the streamwise velocity profiles for turbulent flow with thin entrance boundary layers with reasonable accuracy. For the case of laminar flow with appreciably thicker boundary layers and larger regions of vortex flow, further code refinements are required to achieve quantitative agreement. A third assessment was performed of the ability of the Denton code to predict the rotor exit flow angle distribution and total pressure variation for a radial inflow turbine. The three-dimensional inviscid Denton code yielded exit flow angles that were significantly underturned relative to the experimental data, particularly near the hub surface. In addition, the inviscid rotational approach underpredicted the total pressure ratio change. However, an an overall basis, the computed pressure ratio averaged over the annular height was in good agreement with experimental measurements, provided the rotor inlet angle was adjusted by a few degrees. It is further concluded that the typical blunt leading edges and thick trailing edges of a cooled radial turbine require the inclusion of viscous parameters in the numerical formulation.

The final assessment was on the application of the Navier-Stokes code, MINT, to an axial turbine cascade. This laminar comparison made use of the excellent comparative results obtained for two-dimensional blade pressure distributions and the experimentally observed flow phenomena in turbine passages, i.e., secondary flow patterns. It was concluded that the essential flow physics associated with turbine cascade flow fields were duplicated. Saddle point occurrence, flow-turning, leading edge stagnation region, and boundary layer development were all computed. Further experimental data and code developments are needed in order to carry out a turbulent computation for comparison with experimental data and assessment.

In summary, the ability to compute flow fields within rotors, ducts, and cascades has evolved to a reasonable degree of accuracy, with some exception. In contrast, the ability to predict radial-inflow rotor exit flow is much less accurate with Euler type codes. In view of the highly complex nature of the leading and trailing edge flows, as well as a desire to exploit novel changes such as hub and shroud contouring (14), development of an accurate three-dimensional viscous code is needed.

REFERENCES

1. Povinelli, L.A.: Assessment of Three-Dimensional Inviscid Codes and Loss Calculations for Turbine Aerodynamic Computations. J. Eng. Gas Turbines Power, Vol. 107, April 1985, pp. 265-276.
2. Boyle, R.J.; Haas, J.E.; and Katsanis, T.: Comparison Between Measured Turbine Stage Performance and the Predicted Performance Using Quasi-3D Flow and Boundary Layer Analyses. NASA TM-83640, 1984.
3. Denton, J.D.; and Singh, U.K.: Time Marching Methods for Turbomachinery Flow Calculation. Application of Numerical Methods to Flow Calculations in Turbomachines, Von Karman Institute for Fluid Dynamics, Rhode Saint Genese, Belgium, 1979.
4. Denton, J.D.: An Improved Time Marching Method for Turbomachinery Flow Calculation. ASME Paper 82-GT-239, 1982.
5. Denton, J.D.: A Method of Calculating Fully Three Dimensional Inviscid Flow Through Any Type of Turbomachine Blade Row. Aerothermodynamics of Low Pressure Steam Turbines and Condensers, Vol. 1, Von Karman Institute for Fluid Dynamics, Rhode Saint Genese, Belgium, 1983.
6. Briley, W.R.; and McDonald, H.: Analysis and Computation of Viscous Subsonic Primary and Secondary Flows. AIAA Paper 79-1453, July 1979.
7. Levy, R.; McDonald, H.; Briley, W.R.; and Kreskovsky, J.P.: A Three-Dimensional Turbulent Compressible Subsonic Duct Flow Analysis for Use with Constructed Coordinate Systems. AIAA Paper 80-1398, July 1980.
8. Levy, R.; Briley, W.R.; and McDonald, H.: Viscous Primary/Secondary Flow Analysis for Use with Nonorthogonal Coordinate Systems. AIAA Paper 83-0556, January 1983.
9. Shamroth, S.J.; McDonald, H.; and Briley, W.R.: Prediction of Cascade Flow Fields Using the Averaged Navier-Stokes Equations. J. Eng. Gas Turbines Power, Vol. 106, no. 2, April 1984, pp. 383-390.
10. Pierzga, M.J; and Wood, J.R.: Investigation of the Three-Dimensional Flow Field Within a Transonic Fan Rotor: Experiment and Analysis. J. Eng. Gas Turbines Power, vol. 107, April 1985, pp. 436-449.
11. Strazisar, A.J.: Investigation of Flow Phenomena in a Transonic Fan Rotor Using Laser Anemometry. J. Eng. Gas Turbines Power, vol. 107, April 1985, pp. 427-435.
12. Towne, C.E.: Computation of Viscous Flow in Curved Ducts and Comparison with Experimental Data. NASA TM-83548, 1983.
13. Towne, C.E.; and Schum, E.F.: Application of Computational Fluid Dynamics to Complex Inlet Ducts. NASA TM-87060, 1985.
14. Civinskas, K.C.; and Povinelli, L.A.: Application of a Quasi-3D Inviscid Flow and Boundary Layer Analysis to the Hub-Shroud Contouring of a Radial Turbine. NASA TM-83669, 1984.
15. Choo, Y.K.; and Civinskas, K.C.; Three-Dimensional Inviscid Analysis of Radial Turbine Flow and a Limited Comparison with Experimental Data. NASA TM-87091, 1985.
16. Weinberg, B.C.; Yang, R.J.; McDonald, H.; and Shamroth, S.J.: Calculations of Two and Three-Dimensional Transonic Cascade Flow Fields Using the Navier-Stokes Equations. ASME Paper 85-GT-66, March 1985.
17. Fluegge-Lotz, I.; and Reyhner, T.A.: The Interaction of a Shock Wave With A Laminar Boundary Layer. Int. J. Non-Linear Mechanics, Vol. 3, June 1968, pp. 173-199.
18. McLallin, K.L.; and Haas, J.E.: Experimental Performance and Analysis of 15.04-Centimeter-Tip-Diameter, Radial-Inflow Turbine With Work Factor of 1.126 and Thick Blading. NASA TP-1730, October 1980.
19. Hylton, L.D.; Mihelc, M.S.; Turner, E.R.; Nealy, D.A.; and York, R.E.: Analytical and Experimental Evaluation of the Heat Transfer Distribution Over the Surfaces of Turbine Vanes. NASA CR-168015, May 1983.

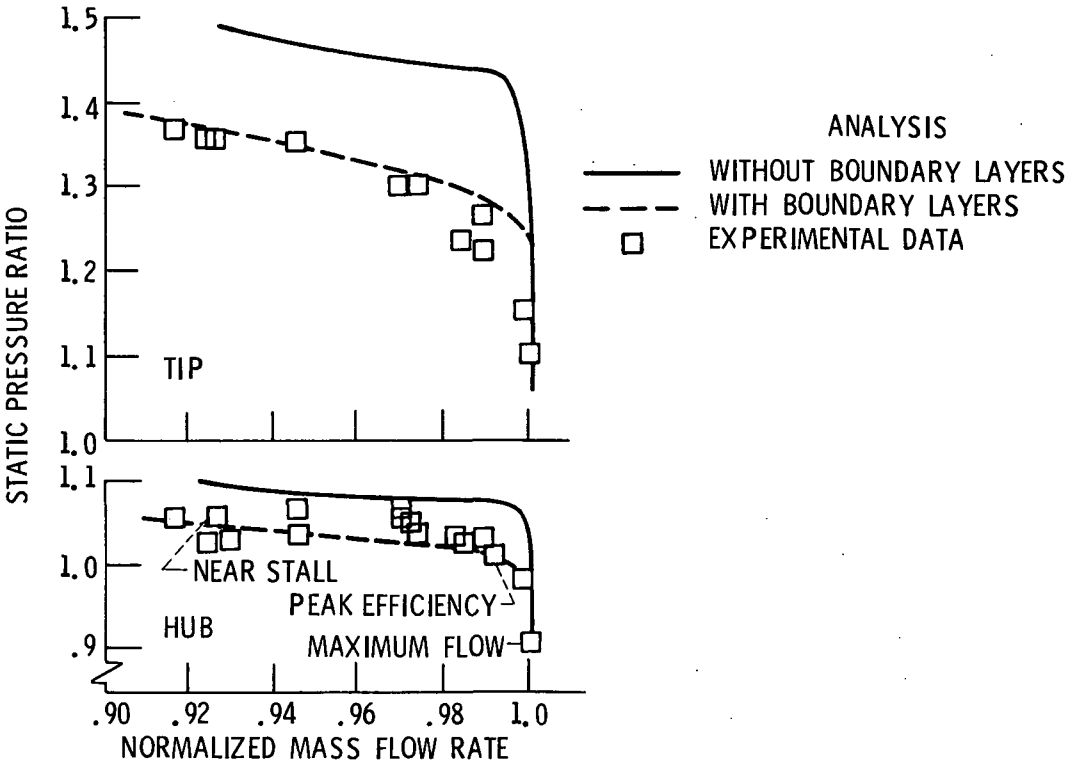

(a) Rotor hub and tip static pressure ratio at design speed.

Figure 1. - Rotor static pressure rise and radial work distribution.

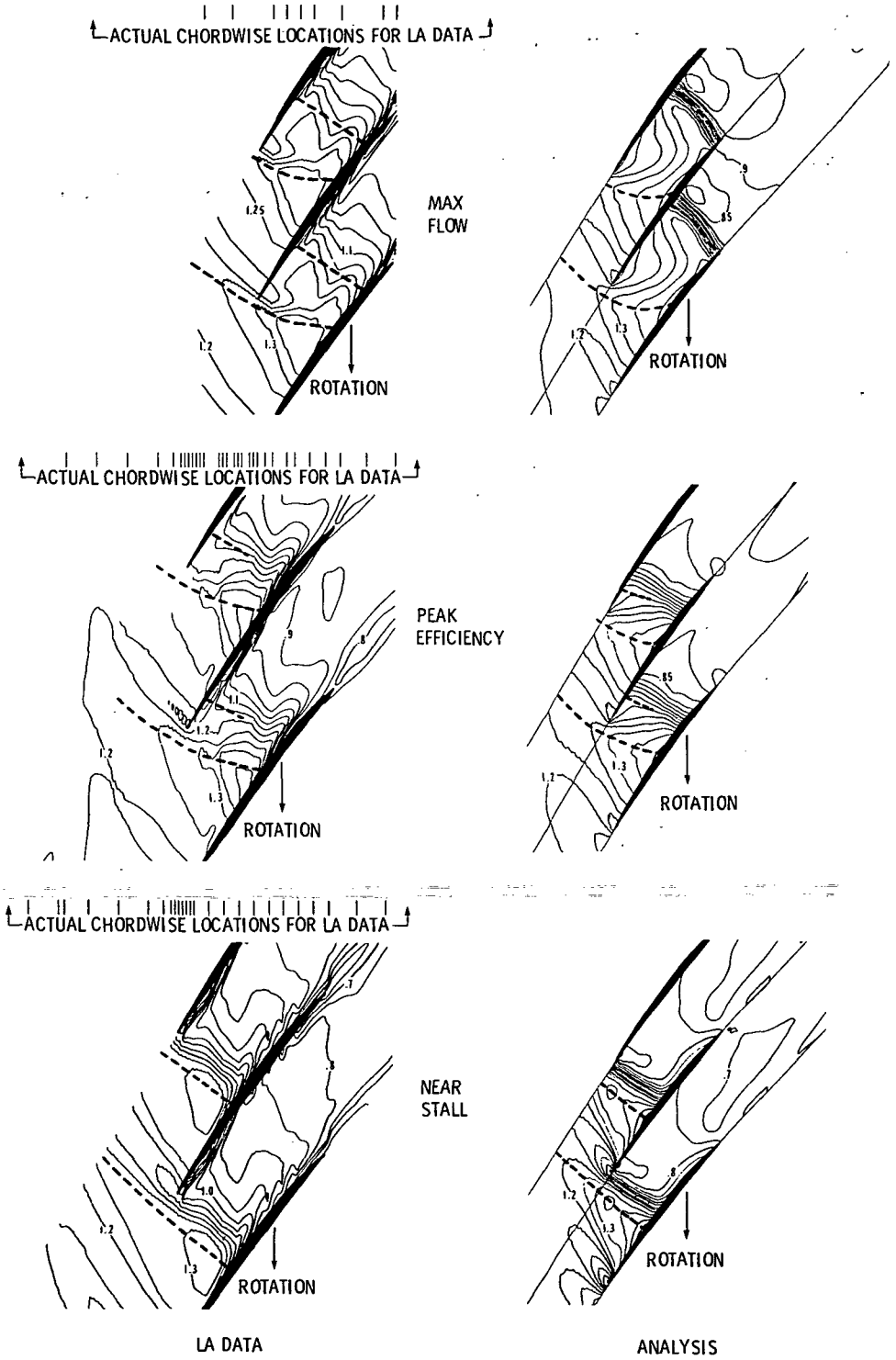

Figure 2. - Contour plots of relative Mach number at 30% span from the tip for max flow, peak efficiency, and near stall flow points: comparison of LA survey results with analysis results. ----Shock location.

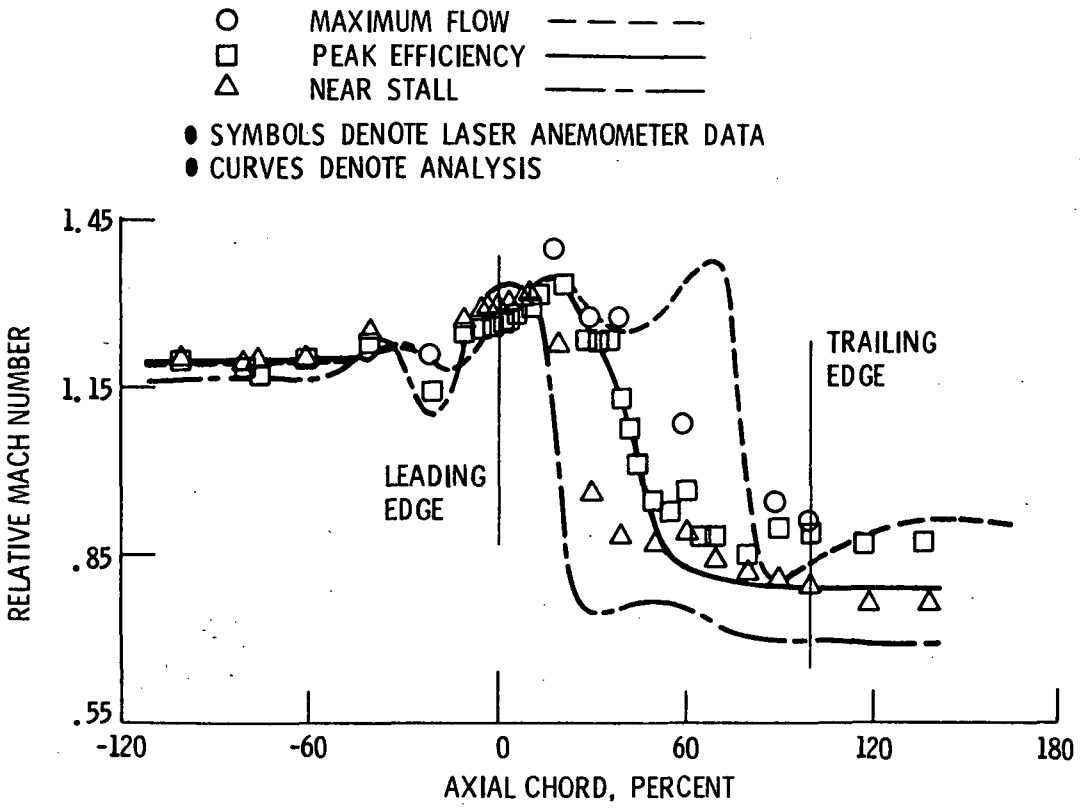

Figure 3. - Variation in relative Mach number with percent chord at mid-pitch for three flow points at 30-percent span from the tip.

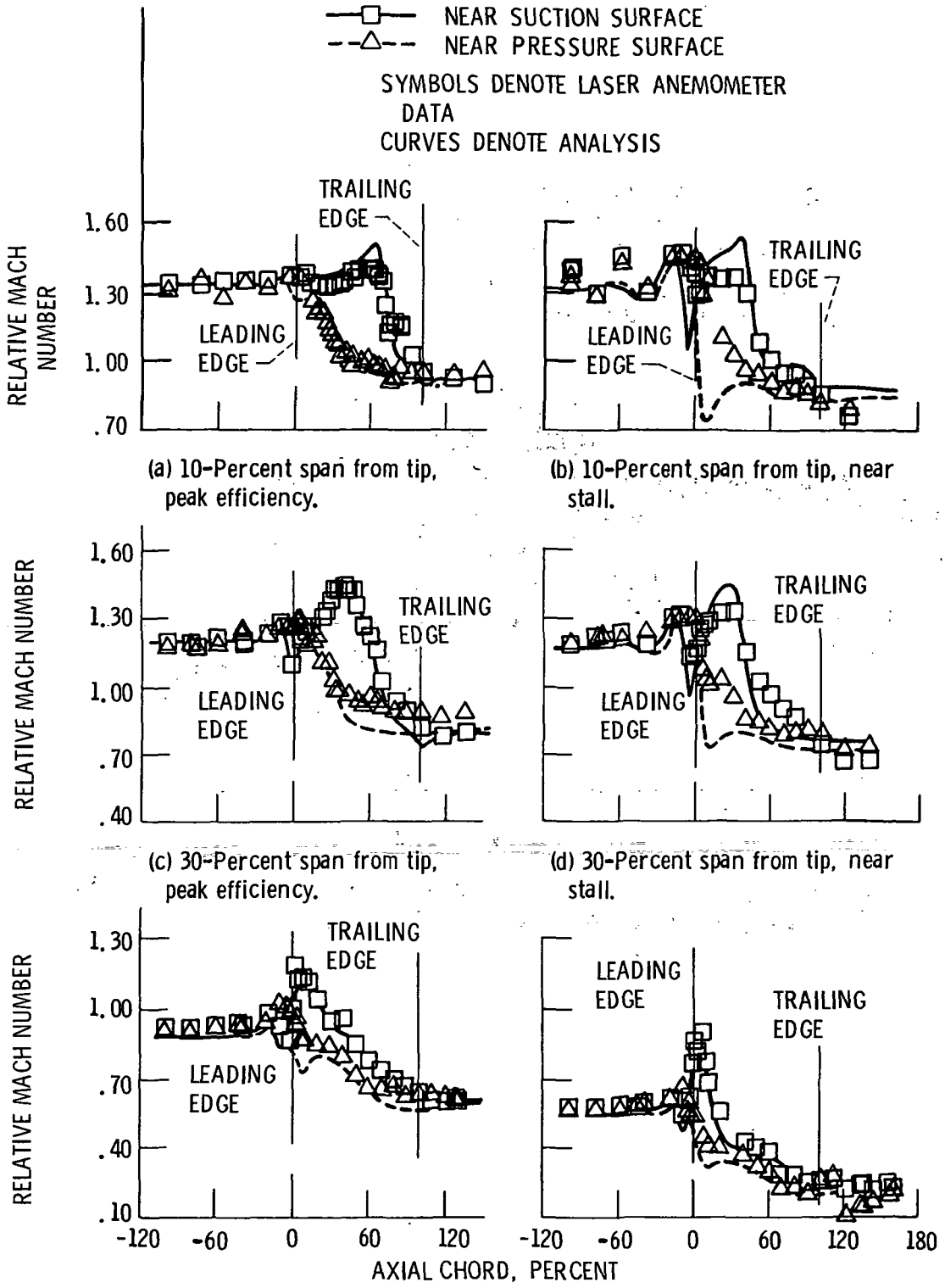

(a) 10-Percent span from tip, peak efficiency.

(b) 10-Percent span from tip, near stall.

(c) 30-Percent span from tip, peak efficiency.

(d) 30-Percent span from tip, near stall.

(e) 70-Percent span from tip, peak efficiency.

(f) 70-Percent span from tip, near stall.

Figure 4. - Variation in relative Mach number with percent chord at three spanwise locations for peak efficiency and near stall flows.

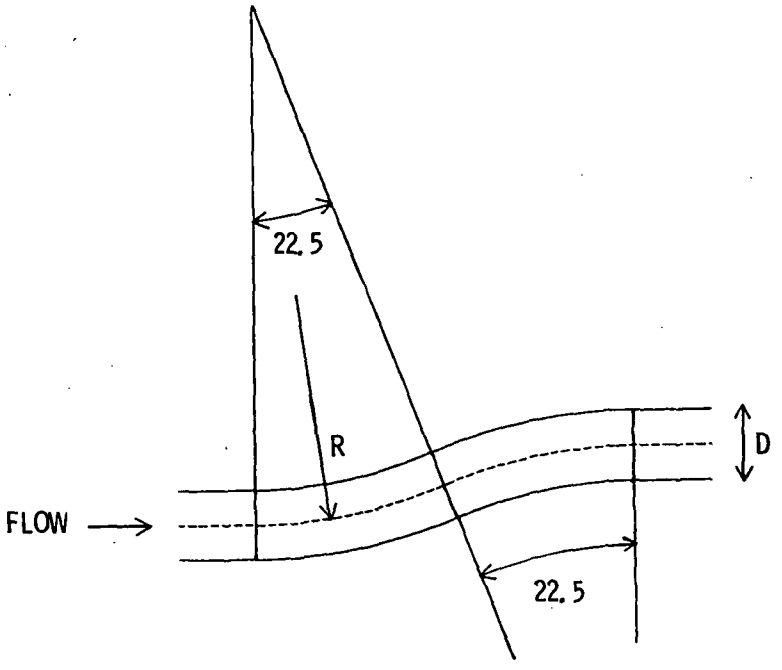

Figure 5. - S-duct configuration.

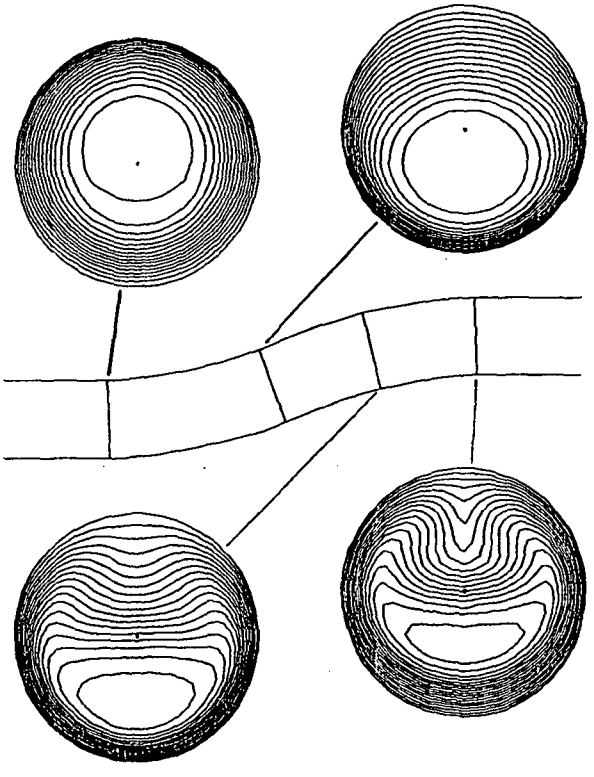

Figure 6. - Computed streamwise velocity contours for laminar flow in 22.5 - 22.5 circular S-duct.

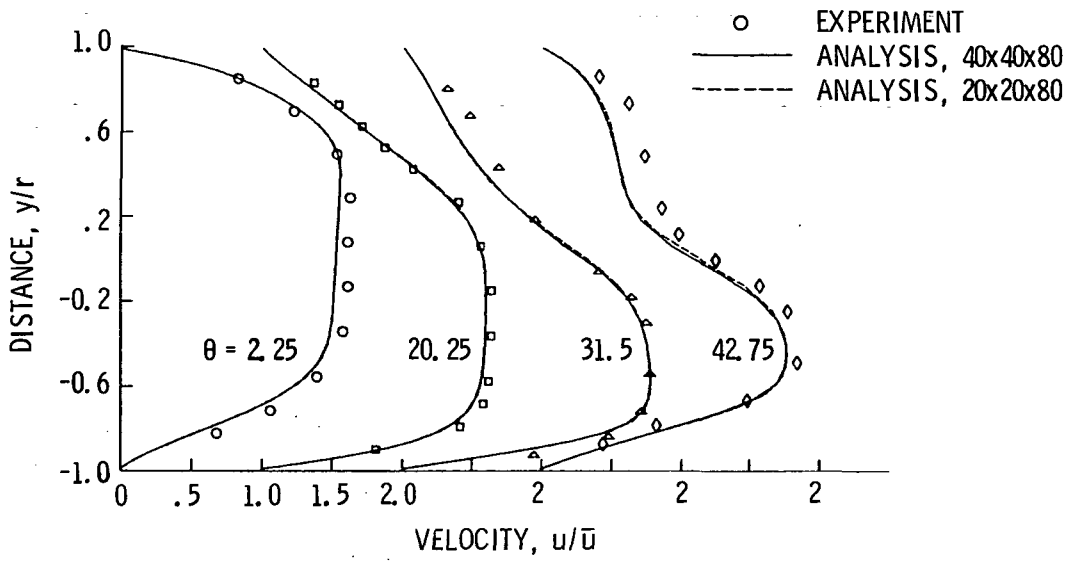

Figure 7. - Computed and experimental streamwise velocity profiles in symmetry plane for laminar flow in 22.5 - 22.5 circular S-duct.

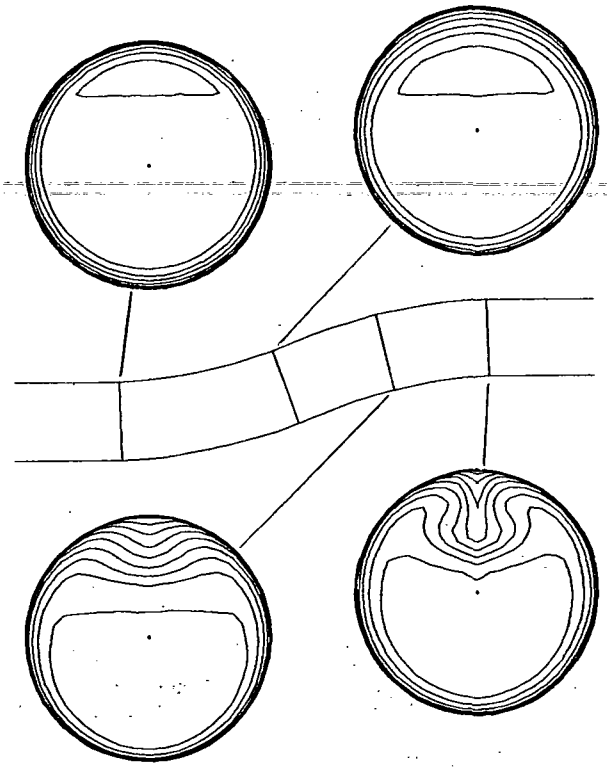

Figure 8. - Computed streamwise velocity contours for turbulent flow in 22.5 - 22.5 circular S-duct.

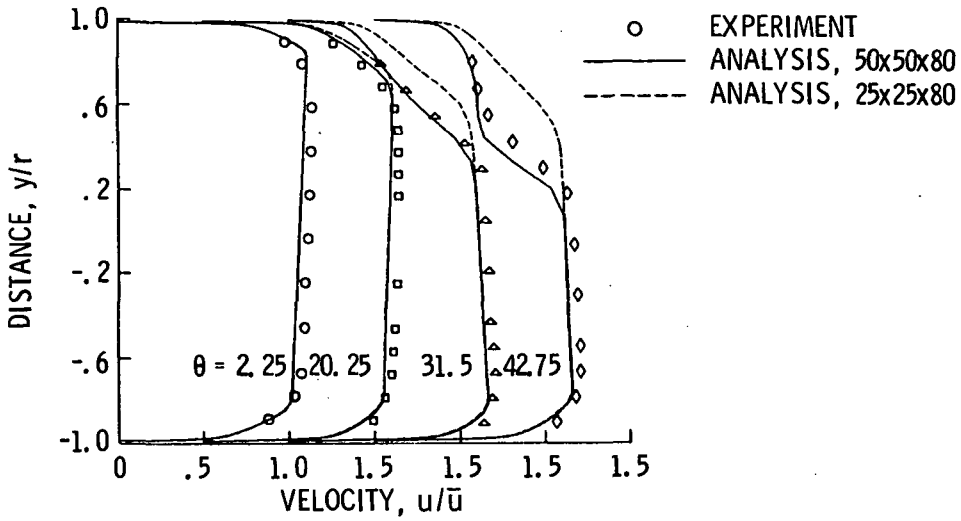

Figure 9. - Computed and experimental streamwise velocity profiles in symmetry plane for turbulent flow in 22.5 - 22.5 circular S-duct.

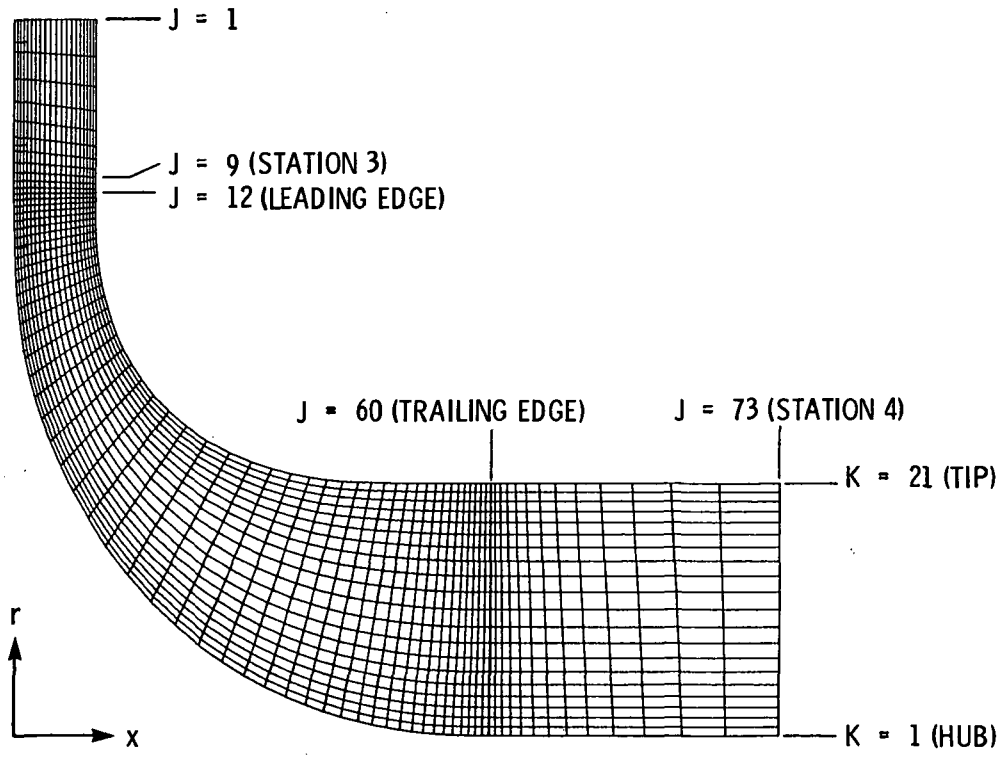

(a) Computational mesh in meridional plane.

Figure 10.

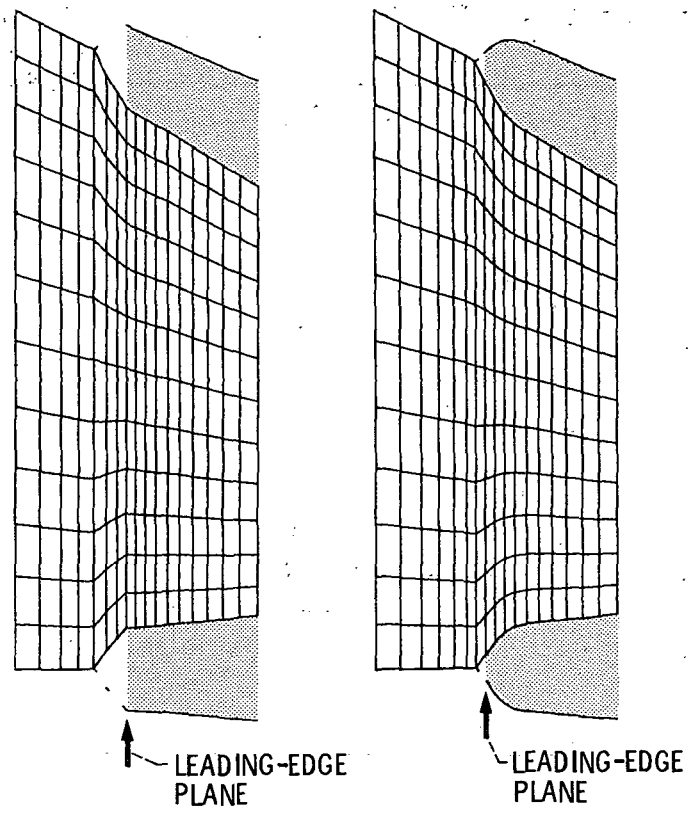

(b) Leading-edge cusps.

Figure 10. - Concluded.

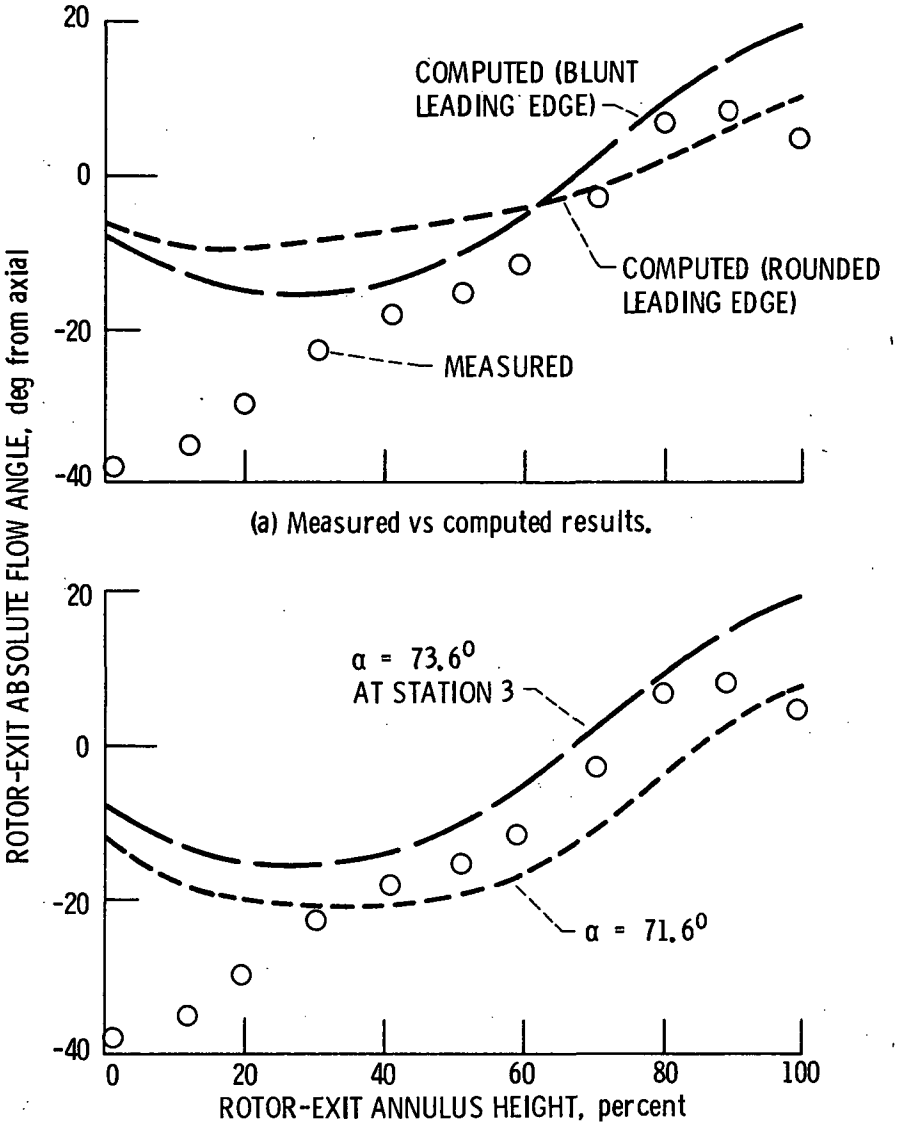

(a) Measured vs computed results.

(b) Effect of rotor-inlet absolute flow angle on the exit absolute flow angle.

Figure 11. - Rotor-exit absolute flow angle.

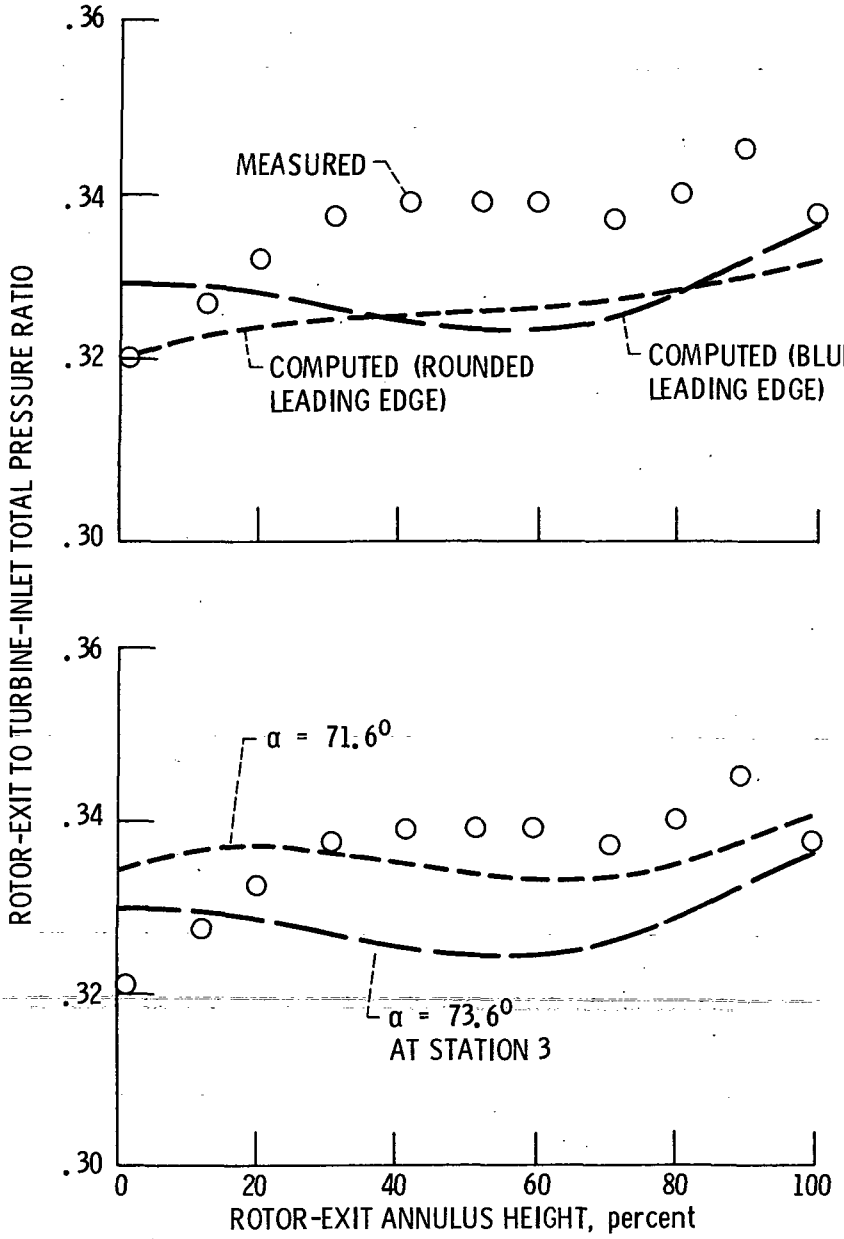

(b) Effects of rotor-inlet absolute flow angle on the total pressure ratio.

Figure 12. - Rotor-exit to turbine-inlet total pressure ratio.

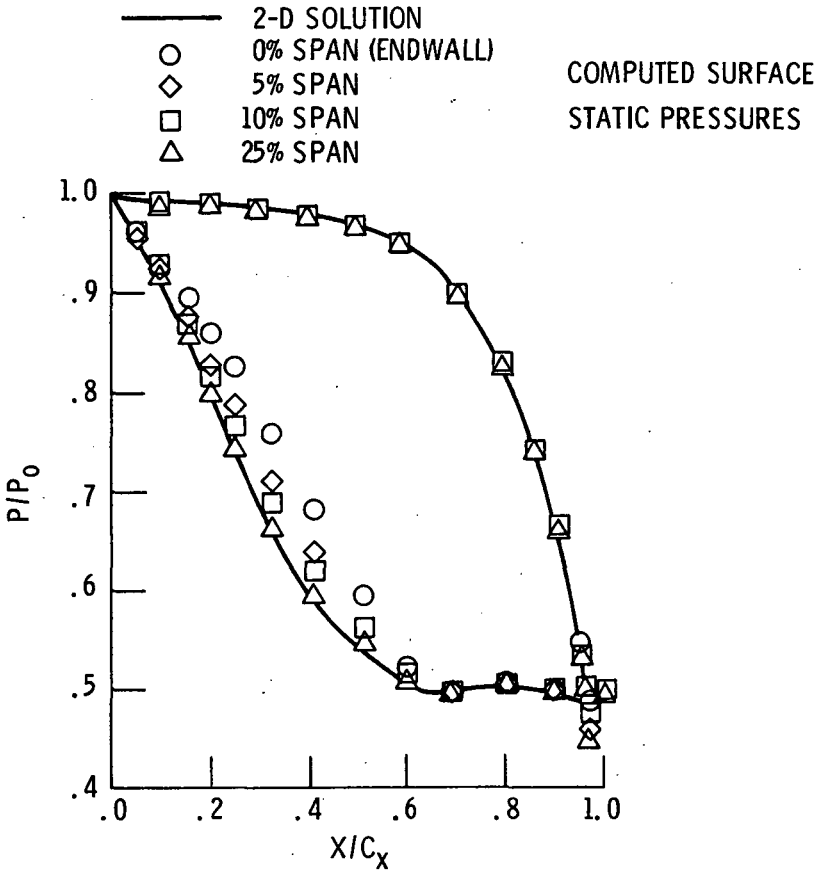

Figure 13. - C3X 3-D Rectilinear cascade pressure coefficient distribution.

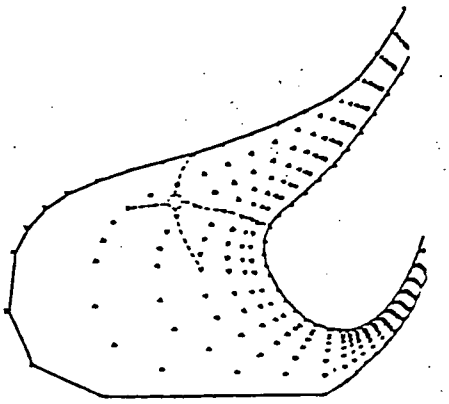

(a) Vector plot on 0.135% spanwise plane.

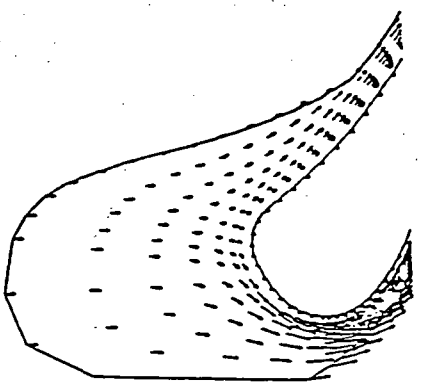

(b) Vector plot on midspan plane.

Figure 14.

1. Report No.	2. Government Accession No.	3. Recipient's Catalog No.
NASA TM-87193		

4. Title and Subtitle	5. Report Date
Validation of Viscous and Inviscid Computational Methods for Turbomachinery Components	
	6. Performing Organization Code: 505-62-21

7. Author(s)	8. Performing Organization Report No.
Louis A. Povinelli	E-2765
	10. Work Unit No.

9. Performing Organization Name and Address	11. Contract or Grant No.
National Aeronautics and Space Administration Lewis Research Center Cleveland, Ohio 44135	
	13. Type of Report and Period Covered: Technical Memorandum

12. Sponsoring Agency Name and Address	14. Sponsoring Agency Code
National Aeronautics and Space Administration Washington, D.C. 20546	

15. Supplementary Notes

Prepared for the 31st International Gas Turbine Conference, sponsored by the American Society of Mechanical Engineers, Dusseldorf, West Germany, June 8-12, 1986.

16. Abstract

An assessment of several three-dimensional computer codes used at the NASA Lewis Research Center is presented. Four flow situations are examined, for which both experimental data and computational results are available. The four flows form a basis for the evaluation of the computational procedures. It was concluded that transonic rotor flow at peak efficiency conditions may be calculated with a reasonable degree of accuracy, whereas, off-design conditions are not accurately determined. Duct flows and turbine cascade flows may also be computed with reasonable accuracy whereas radial inflow turbine flow remains a challenging problem.

17. Key Words (Suggested by Author(s))	18. Distribution Statement
Turbomachinery; Code validation; Aerodynamic analysis	Unclassified - unlimited STAR Category 02

19. Security Classif. (of this report)	20. Security Classif. (of this page)	21. No. of pages	22. Price*
Unclassified	Unclassified		

*For sale by the National Technical Information Service, Springfield, Virginia 22161

National Aeronautics and
Space Administration

Lewis Research Center
Cleveland, Ohio 44135

Official Business
Penalty for Private Use $300

SECOND CLASS MAIL

ADDRESS CORRECTION REQUESTED

Postage and Fees Paid
National Aeronautics and
Space Administration
NASA-451

NASA